# Filling the gap between transient and steady shear rheology of aqueous graphene oxide dispersions

**Rheologica Acta manuscript No.**
(will be inserted by the editor)

# Filling the gap between transient and steady shear rheology of aqueous graphene oxide dispersions

**Francesco Del Giudice[1,5], Benjamin V. Cunning[2], Rodney S. Ruoff[2,3,4], Amy Q. Shen[1]**

[1] Micro/Bio/Nanofluidics Unit, Okinawa Institute of Science and Technology Graduate University, Japan. e-mail: francesco.delgiudice@me.com

[2] Center for Multidimensional Carbon Materials (CMCM), Institute for Basic Science (IBS), Ulsan 44919, Republic of Korea.

[3] Department of Chemistry, Ulsan National Institute of Science and Technology (UNIST), Ulsan 44919, Republic of Korea

[4] School of Materials Science and Engineering, Ulsan National Institute of Science and Technology (UNIST), Ulsan 44919, Republic of Korea

[5] Systems and Process Engineering Centre, College of Engineering, Swansea University, Fabian Way, Swansea SA1 8EN, UK

Received: date / Revised version: date

**Abstract** Even though the rheological behaviour of aqueous graphene oxide (G-O) dispersions has been shown to be strongly time-dependent, only few transient measurements have been reported in the literature. In this work, we attempt to fill the gap between transient and steady shear rheological characterizations of aqueous G-O dispersions in the concentration range of $0.004 < \phi < 3.5$ wt%, by conducting comprehensive rheological measurements, including oscillatory shear flow, transient shear flow, and steady shear flow. Steady shear measurements have been performed after the evaluation of transient properties of the G-O dispersions, to assure steady-state conditions. We identify the critical concentration $\phi_c = 0.08$ wt% (where G-O sheets start to interact) from oscillatory shear experiments. We find that the rheology of G-O dispersions strongly depends on the G-O concentration $\phi$. Transient measurements of shear viscosity and first normal stress difference suggest that G-O dispersions behave like nematic polymeric liquid crystals at $\phi/\phi_c = 25$, in agreement with other work reported in the literature.

G-O dispersions also display a transition from negative to positive values of the first normal stress difference with increasing shear rates. Experimental findings are compared and discussed with models and experiments reported for nematic polymeric liquid crystals, laponite and organoclay dispersions.

**Key words** Graphene Oxide Liquid Crystals 2-D suspensions 2-D dispersions Normal stress Rheology

## 1 Introduction

Graphene oxide (G-O) is an oxidized monolayer of carbon atoms packed in a two dimensional sheet (Dreyer et al (2010); Geim and Novoselov (2007)). G-O contains several reactive oxygen functional groups, and has found applications in a variety of fields due to its excellent mechanical, thermal, and electrical properties (Geim and Novoselov (2007); Park and Ruoff (2009)). Interactions between G-O sheets or between G-O sheets and the suspending liquid result in an enhancement of mechanical properties (Kim and Macosko (2009); Liu et al (2011)). In this regard, G-O serves well in composite materials when it is mixed with polydimethylsiloxane (PDMS) (Guimont et al (2011); Niu et al (2014, 2015)), hydrogels (Liu et al (2011); Das et al (2013); Kim and Lee (2014); Bai et al (2011)), polycarbonate (Kim and Macosko (2009); Potts et al (2011)), polymethylmethacrylate (Tripathi et al (2015)), polyurethane (Sadasivuni et al (2014)), and cellulose (Yao et al (2014)).

The configuration of G-O sheets in a solvent is dramatically affected by its concentration $\phi$ (Vasu et al (2013)). Below a *critical concentration* $\phi_c$, G-O sheets behave like dispersed isolated sheets. When $\phi/\phi_c > 1$, interactions between G-O sheets lead to formation of heterogeneous G-O clusters (Vasu et al (2013); Del Giudice and Shen (2017); Naficy et al (2014)). By increasing the volume concentration further, G-O sheets are reported to become locally more aligned due to inter-particle interactions, displaying some oriented domains surrounded by irregular clusters (Xu and Gao (2011); Kumar et al (2014); Naficy et al (2014)). Such domains are typical of polymeric liquid crystals in the *nematic* phase (Larson (1999)) and of aqueous liquid-crystalline clay suspensions (Michot et al (2006)). Materials with different G-O concentrations $\phi$ exhibit different mechanical properties, which can be characterised rheologically.

Despite its wide use for mechanical characterisations, rheological studies also serve as a powerful tool to determine the relation between local microstructure and macroscopic properties of a given material (Macosko (1994)). The relationship between the local orientation of dispersed materials and macroscopic

properties of the resulting dispersion at both $\phi/\phi_c < 1$ and $\phi/\phi_c > 1$ has been reported for single-walled carbon nanotubes in both aqueous (Hobbie (2010)) and composite materials (Chatterjee and Krishnamoorti (2013)). Basic understanding of micro and macrostructure has been achieved by comparing single-walled carbon nanotubes to rod-like polymer solutions (Green et al (2009); Shaffer and Windle (1999)). The same is not true for G-O dispersions, where a basic understanding has yet to be achieved. Surprisingly, rheology of G-O sheets has never been extensively compared to the rheology of other 2D materials such as laponite (Pignon et al (1997b)) or organoclays (King Jr et al (2007)), to derive a more thorough understanding of the relation between macroscopic properties (rheology) and microstructures of dispersed G-O sheets.

Rheological characterization is usually accomplished by using three representative measurements: *oscillatory shear flow*, *steady shear flow*, and *transient shear flow*. Mechanical properties such as the storage modulus $G'$ and the viscous modulus $G''$ are derived through oscillatory shear measurements, while fluid shear viscosity is measured through steady shear measurements. Transient measurements are necessary to evaluate the time-dependent response of the material, and to determine when the system reaches steady-state conditions.

Current methodologies for the synthesis of G-O sheets lead to G-O sheets with wide size distributions (Dreyer et al (2010)). Because of cluster formation at $\phi/\phi_c > 1$ (Vasu et al (2013); Del Giudice and Shen (2017); Naficy et al (2014)), some precautions need to be taken before proceeding with the determination of the rheological parameters. For example, heterogeneous clusters can disintegrate under a simple shear flow. During shearing, clusters disintegrate and G-O sheets are aligned along the flow direction (Vasu et al (2013); Del Giudice and Shen (2017)). When the flow is arrested, G-O sheets are free to diffuse, eventually forming new clusters. Accordingly, aqueous G-O dispersions can be considered as *thixotropic* material[1], i.e., a time-dependent material. In other words, the initial condition of each sample before each measurement is shear-history dependent. A known and consistent shear-history prior to each measure, the so-called *preshear*, allows comparisons between aqueous G-O dispersions at different concentrations.

[1] According to the definition of Barnes, Hutton and Walters (Barnes et al (1989)), *thixotropy* (verbatim) "is the decrease (in time) of ... viscosity under constant shear stress or shear rate, followed by a gradual recovery when the stress or shear rate is removed."

The literature commonly reports rheological properties of G-O dispersions as a function of the concentration of G-O sheets $\phi$. To account for different material preparations, we report available results in terms of *dimensionless concentration* $\phi/\phi_c$. Vasu et al (2013) performed rheological characterization of aqueous G-O dispersions at $0.27 < \phi/\phi_c < 80$ (with $\phi_c$=0.038 vol%). They found the existence of the *yield stress* $\tau_y$ for dispersions at $\phi/\phi_c > 1$. Their transient measurements showed that at $\phi/\phi_c = 20$ and at applied shear stress below $\tau_y$, shear viscosity displayed strong temporal oscillations without reaching a steady-state. When increasing the applied stress above $\tau_y$, oscillations disappeared, and the shear viscosity reached steady-state. They also performed oscillatory shear measurements, reporting $G' > G''$ when $\phi/\phi_c > 1$, and $G' < G''$ when $\phi/\phi_c < 1$. However, Vasu et al (2013) did not report transient measurements of shear viscosity at different concentrations, nor did they compare transient and steady shear measurements at different $\phi/\phi_c$. Tesfai et al (2013) focused, instead, on dilute G-O dispersions, with volume fractions $0.005 < \phi < 0.05$ wt% (they did not provide the critical concentration for their G-O dispersion). They reported a weak shear-thinning at $\dot{\gamma} < 100\ s^{-1}$ for concentrations $\phi > 0.03$ wt%, and the infinite-shear viscosity $\eta_\infty$ increased with the increasing concentration. In addition, they found good agreement between their experimental data and the model for dilute suspension of rigid spheres (Krieger and Dougherty (1959)). However, no information on the initial conditions was provided, nor were transient measurements reported. More recently, Vallés et al (2014) performed rheological characterization of aqueous G-O dispersion with $1 < \phi/\phi_c < 267$. As an initial condition, they waited 60 minutes after the dispersions loading. Their results were analogous to previous works (Vasu et al (2013); Tesfai et al (2013)), but no transient measures were performed. Kumar et al (2014) observed a non-monotonic behaviour of the shear viscosity at a fixed shear rate by increasing the concentration of the G-O dispersion, when $0.6 < \phi/\phi_c < 1.2$ (with $\phi_c$ =0.33 vol%). They attributed such behaviour to the shear-induced transition from isotropic to nematic phase in the G-O dispersion, around $\phi_c$, in agreement with the experimental findings of Xu and Gao (2011). However, they did not perform any transient rheological measurements. Very recently, Liu et al (2015) reported transient shear viscosity for G-O dispersions with $0.75 < \phi/\phi_c < 3$ (with $\phi_c$ =0.8 wt%), at a fixed shear rate $\dot{\gamma} = 100\ s^{-1}$, for a measurement duration of 120 s, without employing any preshear or resting time. They found that a clear steady state was never reached, but unfortunately, measurements longer than 120 s were not available.

Even though the rheology of aqueous G-O dispersions has been shown to be strongly time-dependent, only a few transient measurements are reported in the literature. A systematic rheological investigation considering both transient and shear measurements can provide new insights on the relation between local microstructure and macroscopic properties of G-O dispersions. However, to the best of our knowledge, no such studies have been reported.

In this work, we attempt to fill the gap between transient and steady shear rheology of aqueous graphene oxide dispersions. We consider aqueous G-O dispersions in the concentration range of $0.004 < \phi < 3.5$ wt%, being characterised using oscillatory shear flow, transient shear flow over 600 s, and steady shear flow. Oscillatory shear measurements have been used to evaluate viscous and elastic properties of the dispersions, and to determine the critical concentration $\phi_c = 0.08$ wt%, covering the range of dimensionless concentrations $0.05 < \phi/\phi_c < 44$. Prior to each measurement, a preshear $\dot{\gamma} = 1600\ s^{-1}$ for 180 s has been employed in order to impose a consistently defined shear-history for all samples. Transient measurements allow us to determine the steady-state conditions, which are subsequently used for steady shear measurements.

We also report transient and steady shear measurements of the first normal stress difference $N_1$, for G-O dispersion with $\phi/\phi_c = 25$. These results are compared with theories and experiments reported in the literature for nematic polymeric liquid crystals. We also discuss and compare our findings with those available in the literature for other 2D systems such as laponite, kaolin, and other organoclay dispersions.

## 2 Materials and Methods

### *2.1 Sample preparation*

A graphene oxide dispersion at $\phi = 0.4$ wt% was obtained by simply adding G-O sheets (GrapheneA, Spain) to distilled water. G-O dispersions at $\phi = 3.5$ wt% and $\phi = 2$ wt% were obtained by placing hydrogel beads into the G-O at 0.4 wt% to selectively remove water, resulting in dispersions at high concentration, following a methodology reported elsewhere (Akbari et al (2016)). Concentrations of $\phi = 3.5$ wt% and $\phi = 2$ wt% dispersions were measured by UV adsorption. Three stock samples were then prepared: (i) $\phi = 3.5$ wt%, (ii) $\phi = 2$ wt%, (iii) $\phi = 0.4$ wt%. Concentrations $\phi < 0.4$ wt% were prepared by diluting the sample (iii) with distilled water, on a precision balance. We investigated the concentration

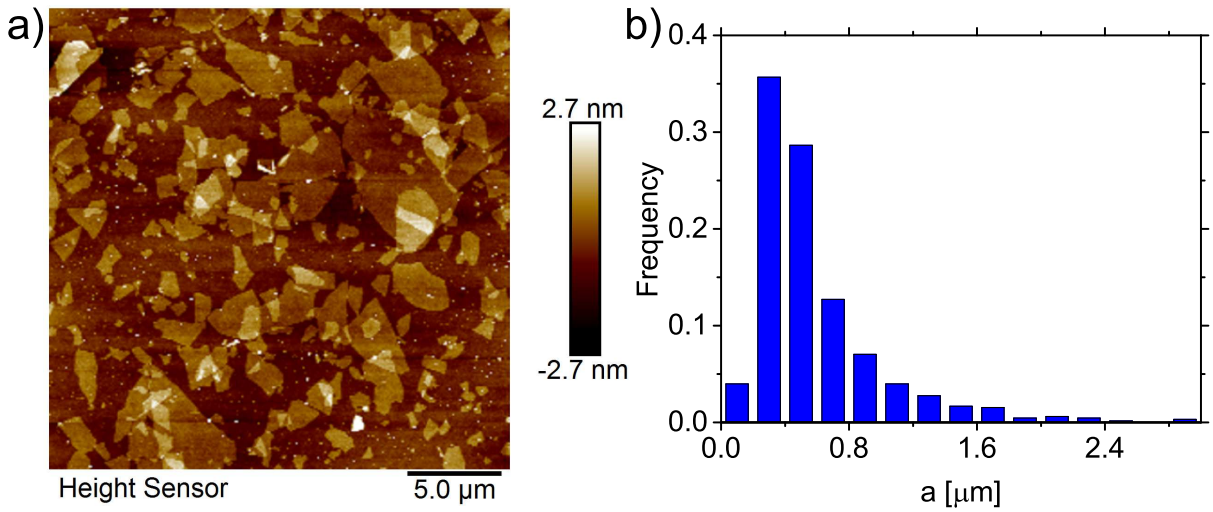


**Fig. 1 G-O sheets display an heterogeneity of size distribution** (a) AFM image of G-O sheets, where the heterogeneity of the material in terms of the lateral radius $a$ is evident. The image was derived in tapping mode by using a 8 nm tip. The thickness of G-O sheets is $d \sim 1$ nm. (b) Distribution of the lateral radius $a$, based on the evaluation of the sheets' area of (a) and other images (not reported). Lateral radius $a$ has been derived by assuming a circular shape for the G-O sheet, thus $a = \sqrt{\text{area}/\pi}$. The parameter $a$ can be regarded as the hydrodynamic radius for a circular object. The average lateral radius is $a = 0.58 \pm 0.40$ $\mu$m.

range $0.004 < \phi < 3.5$ wt%, which corresponds to $0.05 < \phi/\phi_c < 44$, with $\phi_c = 0.08$ wt% (see details in Section 3.1.1).

### *2.2 AFM characterization of G-O sheets*

Statistical analyses and characterisation of G-O sheets were performed using Atomic Force Microscopy (AFM, Bruker Dimension Icon), to determine the sheet lateral size distribution. A square piece ($1 \times 1$ cm$^2$) of silicon wafer with a native oxide layer was subjected to oxygen plasma to make the surface hydrophilic. Then, a diluted G-O dispersion at $\phi \sim 0.04$ wt% was spin coated (500 rpm for 60s) and allowed to dry. A Bruker Dimension Icon AFM instrument in tapping mode with an 8 nm tip was used to image the surface topography of the graphene oxide platelets coated on the silicon wafer. Across 9 scans ($50 \times 50$ $\mu$m$^2$), a total of 653 sheets were analysed. We confirmed the robustness of our statistical analysis by comparing the size distribution of the complete sample (653 sheets) with that of subsets of 100 random sheets.

G-O sheets appear to be very heterogeneous both in their sizes and shapes, and no clear evaluation of the lateral size could be realised (Figure 1a). We then derived the average lateral radius $a$ as follows. Non-overlapping G-O sheets were traced from the raw AFM images using Adobe Photoshop, and further

analyzed with ImageJ (NIH software). The area of each isolated G-O sheet was evaluated in ImageJ. We approximated the area of each sheet as that of a circle, and extracted the lateral radius $a = \sqrt{\text{area}/\pi}$. The parameter $a$ can be regarded as the hydrodynamic radius for a circular object. We then performed a frequency count for each radius $a$, and subsequently evaluated the distribution of lateral radii $a$ (Figure 1b). The average lateral radius is $a = 0.58 \pm 0.40$ $\mu$m. The thickness of G-O sheets measured from AFM images is $d \sim 1$ nm. The measured G-O sheet thickness value agrees well with existing reports (Vasu et al (2013); Vallés et al (2014); Kumar et al (2014); Xu and Gao (2011)). The lateral dimensions of G-O sheets also depends on the sample preparation method. We have estimated the "size" of the G-O sheets by measuring their area, and fitting this area to a circle; thus a single radius is fit for each sheet area measured. The radius values fall in the reported range of 0.3 $\mu$m $< a <$ 2 $\mu$m. For example, $a \sim 2$ $\mu$m was reported by Vasu et al (2013), $a \sim 0.3$ $\mu$m by Vallés et al (2014), $a \sim 0.35$ $\mu$m by Kumar et al (2014), and $a \sim 1$ $\mu$m by Xu and Gao (2011).

### *2.3 Measurements of pH and ζ-potential*

We evaluated the pH (pH-meter, Horiba Scientific) and the ζ-potential (ELSZ-2000, Otsuka Electronics) of aqueous G-O dispersions at different concentrations $\phi/\phi_c$ (Table 1). The pH measurements confirm the acidity of G-O sheets when suspended in water (Li et al (2008)), while ζ-potential measurements show that G-O sheets are negatively charged.

| $\phi/\phi_c$ | pH | ζ-potential [mV] |
|---|---|---|
| 25 | 5.15 | Sample too dark |
| 5 | 2.23 | Sample too dark |
| 2.5 | 2.16 | -20.98±1.62 |
| 1.25 | 2.55 | -32.43±1.92 |
| 1 | 2.76 | -29.76±2.22 |
| 0.5 | 3.00 | -23.16±1.18 |
| 0.25 | 2.445 | -27.03±0.85 |
| 0.1 | 4.5 | -29.29±0.26 |

**Table 1 The pH of aqueous G-O dispersions depends on the G-O concentration, effectively $\phi/\phi_c$.** Measurements of pH and ζ-potential for G-O dispersions in the range of $0.1 < \phi/\phi_c < 25$, with $\phi_c = 0.08$ wt%.

*2.4 Rheological measurements*

Rheological characterization was primarily carried out using a stress controlled shear rheometer (Anton Paar MCR 502). The temperature was fixed at 22°C. Evaporation of aqueous G-O samples was controlled by using a solvent trap. A preshear $\dot{\gamma} = 1600\ s^{-1}$ for 180 s was applied prior to each measurement. A 50 mm stainless-steel parallel-plate geometry with gap size of 200 $\mu$m was used for all experiments, except for the measurement of the first normal stress difference $N_1$.

Transient measurements of the first normal stress difference $N_1$ at $\phi/\phi_c = 25$ were carried out using a strain-controlled shear rheometer (ARES G2, TA instrument) with a cone and plate configuration (50 mm stainless steel with an angle of 0.02 rad).

At high shear rates, inertia of the instrument affects the measurement of the first normal stress difference (Macosko (1994)). In particular, inertial forces pull the two plates together rather than push them apart, leading to a fictitious negative normal force. This force can be modeled as $F_{N,inertia} = -0.075\pi\rho\Omega^2R^4$ (Macosko (1994); Walters (1975)), where $\rho$ is the fluid density, $\Omega$ is the angular velocity and $R$ is the radius of the cone. We also carried out measurements of the normal force $F_N$ for water, which is expected to be null. However, we find residual negative normal force for the water, in the whole range of shear rate investigated $0.01 < \dot{\gamma} < 1000\ s^{-1}$ (See Figure S1). We then used the values of normal force found for the water as calibration for our normal force measurements with G-O at $\phi/\phi_c = 25$, at each shear rate investigated. Note that initial squeezing of the sample between the cone and plate can lead to a positive residual force, which may never relax (Cocchini et al (1992)). We then monitored the normal force after the squeezing of G-O at $\phi/\phi_c = 25$, and found that the residual force approached a steady-state value $F_{N,residual} = 0.4$ N after $\sim 1$ hour (See Figure S2). The transducer was subsequently reset to zero. It is worthwhile to notice that, for the strain-controlled rheometer ARES G2, the detection limit of the normal force is $F_{N,limit} = 0.02$ N, 20 times smaller than the detected residual force $F_{N,residual} = 0.4$ N. Therefore, our measurements are above the detection limit of the rheometer. Transient measurements of $N_1$ over 600 seconds were then carried out in the range of shear rates $0.01 < \dot{\gamma} < 1000\ s^{-1}$, after 1 hr from the squeezing of the sample, without preshear conditions. Finally, transient measurements of $N_1$ carried out using cone and plate geometry can also be affected by the axial response time of the transducer $t_a = 6\pi R\eta/K_A\alpha^3$ (Schweizer and Bardow (2006)), where $R$ is the radius of the sample, $\eta$ is the shear viscosity, $K_A$ is the rheometer axial stiffness, and $\alpha$ is the cone angle. The values of $N_1$ is

not affected by the axial response of the transducer when the experimental time $t$ is longer than $t_a$, i.e., $t/t_a >> 1$ (Schweizer and Bardow (2006)). For G-O at $\phi/\phi_c = 25$, the highest value of $t_a$ is obtained at the lowest shear rate investigated $\dot{\gamma} = 10^{-2}$ s$^{-1}$ (due to the highest value of the shear viscosity $\eta$). By using $R = 25$ mm, $\eta = 1440$ Pa·s, $K_A = 2$ N/$\mu$m (Schweizer and Bardow (2006)), and $\alpha = 0.02$ rad, the resulting axial response time is estimated to be $t_a = 42.4$ s. Our experimental time is $t = 600$ s, thus $t/t_a >> 1$. Therefore, our measurements are not expected to be affected by the axial response time of the rheometer. In summary, measurements of $N_1$ for G-O at $\phi/\phi_c = 20$ were carried out by i) squeezing the sample between cone and plate; ii) waiting 1 hour to stabilize the residual normal force; iii) acquiring the experimental data for every shear rate $\dot{\gamma}$ in the range $0.01 < \dot{\gamma} < 1000\ s^{-1}$; iv) correcting the experimental data from the fictitious inertial force; v) further correcting the experimental data based on the calibration curve for water.

## 3 Experimental Results and Discussion

### *3.1 Oscillatory shear measurements*

*3.1.1 Determination of the critical concentration $\phi_c$* The microstructure of G-O dispersion varies as a function of G-O concentrations and flow properties (Del Giudice and Shen (2017); Naficy et al (2014)). When $\phi/\phi_c < 1$, G-O sheets can be regarded as individual sheets not interacting with adjacent sheets. In this case, the configuration of dispersed G-O in an aqueous media is that of single sheets with different sizes, depending on the lateral radius distribution. When $\phi/\phi_c \sim 1$, G-O sheets interact with adjacent sheets, and agglomerate in heterogeneous clusters. Each cluster is different because it consists of different G-O sheets with different lateral radius. Therefore, the critical concentration is a very important parameter that needs to be determined. Unfortunately, the high standard deviation of G-O lateral radius $a$ makes it difficult to determine $\phi_c$ with existing theoretical models using arguments such as the percolation threshold (Lu and Mai (2005)), Onsager's theory (Onsager (1949)), or isotropic-nematic transition in polymeric liquid crystals (Aboutalebi et al (2011); Eppenga and Frenkel (1984)). Here, we determined $\phi_c$ by using oscillatory shear measurements, which also provided the storage modulus $G'$ and the viscous modulus $G''$ of G-O dispersions (Figure 2a). When $\phi/\phi_c < 1$, aqueous G-O dispersions behave like a dispersion of single sheets; thus, elastic modulus is expected to be negligible with respect to the viscous modulus, i.e., $G' < G''$. By increasing the G-O concentration, clusters are formed, and the elastic com-

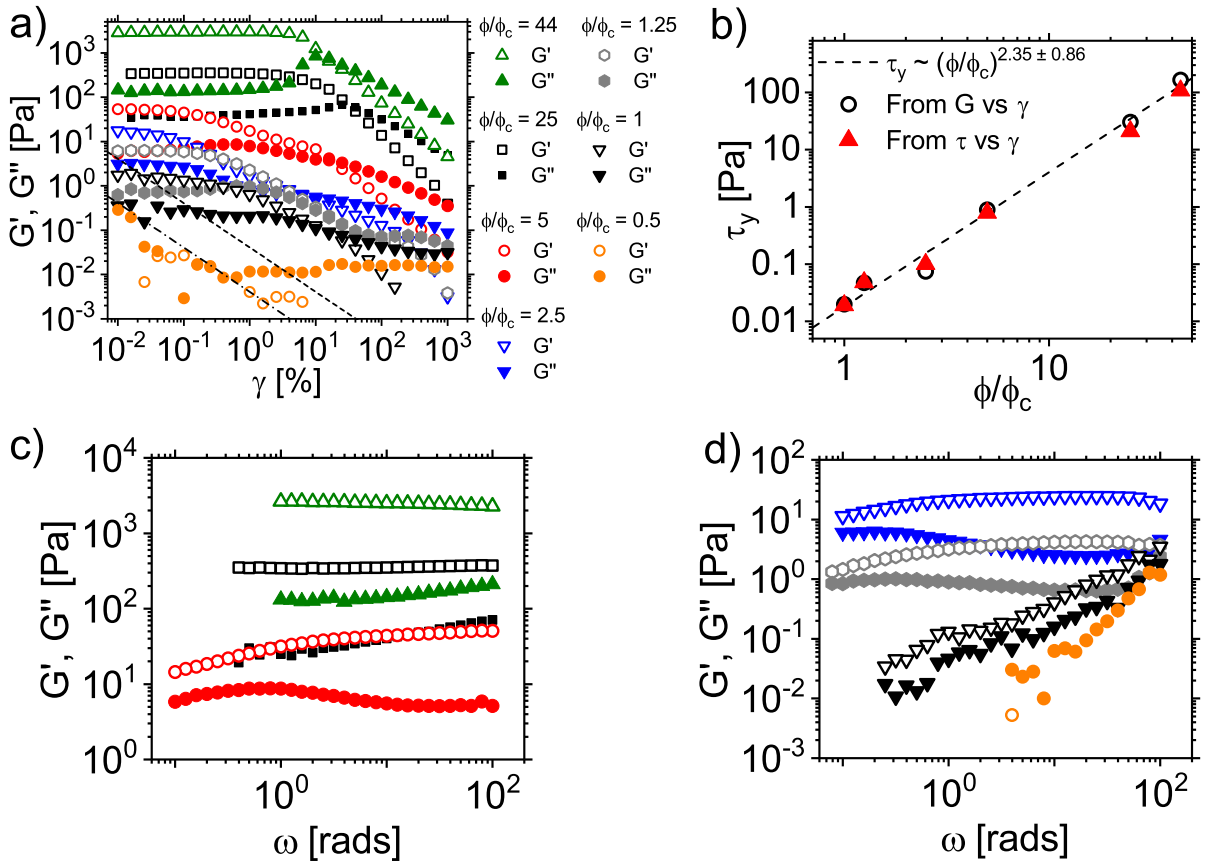


**Fig. 2 G-O dispersions show elasticity and yield stress above the critical concentration $\phi_c$.** (a) Storage modulus $G'$ and loss modulus $G''$ as a function of the imposed deformation $\gamma$ (amplitude sweep experiment), with an imposed angular frequency $\omega = 10$ rad/s, for dispersions of G-O sheets at concentrations $0.5 < \phi/\phi_c < 44$, with $\phi_c = 0.08$ wt%. Dashed-dotted line and dashed lines represent the minimum value of modulus $G_{min}$ detectable by the rheometer (due to the low-torque limit, as reported by Macosko (1994); Ewoldt et al (2015)), $G_{min} = 2T_{min}/(\pi R^3 \gamma)$, where $T_{min}$ is the minimum torque detectable, $R = 25$ mm is the plate diameter, and $\gamma$ is the amplitude. Dashed line is $G_{min}$ for $T_{min} = 1$ $\mu$N·m, while dashed-dotted line is $G_{min}$ for $T_{min} = 0.1$ $\mu$N·m (b) Estimates of the yield stress $\tau_y$ from both amplitude sweep measurements with the condition $G' = G''$ at each $\phi/\phi_c$ (black open circles), and from the same data set plotted as total stress $\tau$ versus amplitude $\gamma$ (red triangle). In the last case, the yield stress $\tau_y$ is evaluated from the change of the slope of $\tau$ (Figure S3). Dashed line is the best fit $\tau_y \propto (\phi/\phi_c)^{2.35\pm0.86}$. (c-d) Storage modulus $G'$ and loss modulus $G''$ as a function of the angular frequency $\omega$ with an imposed deformation $\gamma = 0.1$ % (frequency sweep experiment), for dispersions of G-O sheets at concentrations $5 < \phi/\phi_c < 44$ (c), and $0.5 < \phi/\phi_c < 2.5$ (d), with $\phi_c = 0.08$ wt%. Symbols in (c-d) are the same as those shown in (a). A preshear $\dot{\gamma} = 1600$ $s^{-1}$ for 180 s is applied prior to each measurement.

ponents become stronger than the viscous components, i.e., $G' > G''$. The critical concentration $\phi_c$ can then be estimated through the transition from viscous-dominated to elastic-dominated behaviour. Similar

rheological approach was also employed by King Jr et al (2007) for the evaluation of the critical concentration of organoclay dispersions. The critical concentration based on the oscillatory shear measurement is identified as $\phi_c = 0.08$ wt%. Notice that positive values of $G'$ are found also at $\phi = 0.04$ wt%. However, at $\phi = 0.04$ wt% we are below the sensitivity of the rheometer for the measurement of $G'$. The minimum value of modulus $G_{min}$ (either $G'$ or $G''$) dictated by the low-torque limit can be evaluated for parallel plate geometry as (Macosko (1994); Ewoldt et al (2015)):

$$G_{min} = \frac{2T_{min}}{\pi R^3 \gamma}, \tag{1}$$

where $T_{min}$ is the minimum torque detectable, $R = 25$ mm is the plate diameter, and $\gamma$ is the amplitude (Figure 2a) . Dashed line of Figure 2a is $G_{min}$ for $T_{min} = 1$ $\mu$N·m, while dashed-dotted line is $G_{min}$ for $T_{min} = 0.1$ $\mu$N·m. For our rheometer (Anton Paar MCR502), the lowest detectable torque by technical specification is $T_{min} = 0.1$ $\mu$N·m (dashed-dotted line in Figure 2a). However, a more conservative value for the torque is $T_{min} = 1$ $\mu$N·m (dashed line in Figure 2a). Therefore, $\phi_c = 0.08$ wt% can be considered as a good estimate of the critical concentration.

*3.1.2 Determination of the viscoelastic properties* Amplitude sweep measurements allow the determination of $G'$ and $G''$ as a function of the imposed deformation $\gamma$, at an imposed frequency $\omega$. This measurement first identifies the so-called linear regime (where $G'$ and $G''$ are independent of $\gamma$). At $\gamma = 0.1$ % and $\phi/\phi_c > 1$, we observe $G' > G''$ (Figure 2a), in agreement with previous findings (Vallés et al (2014)). At $\phi/\phi_c = 44$, storage and loss moduli are parallel and independent of the imposed deformation for $\gamma < 10$ %. Around $\gamma \sim 10$ %, $G' = G''$, and the viscous component overcomes the elastic one when $\gamma > 10$ % (non-linear regime). The same trend is found at concentrations down to $\phi/\phi_c = 1$. For a fixed concentration, we observe a transition from elastic to viscous dominated behaviour. Since the elastic-dominated behaviour is related to the formation of clusters, the viscous-dominated behaviour can be reasonably ascribed to the separation of such clusters. Another transition point can then be estimated when $G' = G''$, for each fixed concentration. The deformation $\gamma$ at which $G' = G''$, is linked to a specific shear stress $\tau$ imposed on the aqueous dispersions. The stress at which $G' = G''$ in amplitude sweep measurements offers a good estimate of the *yield stress* $\tau_y$ (Figure 2b) (Shih et al (1999); Kugge et al (2011); Perge et al (2014); Renou et al (2010)). A different way to measure the yield stress was also recently reported by Dinkgreve et al (2016). In their study, the yield stress $\tau_y$ was estimated as the point

at the onset of the slop change in a $\tau - \gamma$ plot (Figure S3), where $\gamma$ is the deformation and $\tau$ is the total stress. The values of $\tau_y$ measured through this technique are in very good agreement with our previous estimate (see red triangle in Figure 2b). Our yield stress values scale with the dimensionless concentration as $\tau_y \propto (\phi/\phi_c)^{2.35\pm0.86}$, in very good agreement with the scaling exponent $2.5 \pm 0.1$ found by Vasu et al (2013) and 2.86 reported by Kumar et al (2014). Pignon et al (1997b) studied dispersions of laponite, whose morphologies and inter-particle interactions are comparable to G-O sheets. They reported the scaling $\tau_y \propto \phi^2$ near $\phi_c$, while $\tau_y \propto \phi^3$ at higher concentrations. King Jr et al (2007) fitted their data in the whole concentration range with $\tau_y \propto \phi^3$ for organoclays dispersed in water. However, their raw data displayed a concentration-dependent transition between two regimes. Remarkably, the scaling found in their range of volume fractions $0.011 < \phi < 0.045$ led to $\tau_y \propto \phi^{2.43\pm0.1}$, in excellent agreement with our findings, and with those reported by Vallés et al (2014) and Kumar et al (2014). Our values of $\tau_y$ are also in good agreement with those reported by Vasu et al (2013) and in rather good agreement with those of Kumar et al (2014), in the same range of $\phi/\phi_c$.

The presence of a yield stress when $\phi/\phi_c > 1$ is a fingerprint of G-O sheets network formation. It is then natural to ask whether G-O sheets form "house-of-cards" (disordered) or "edge-to-edge" (ordered parallel sheets, typical for the nematic polymeric liquid crystals) structures, analogous to the case of clay dispersions (Benna et al (1999)), at $\phi/\phi_c > 1$. In this respect, the literature dealing with the rheology of clay dispersions generally acknowledged the strong dependence of the rheology on the pH of clay dispersions. Khandal and Tadros (1988) found that the storage modulus $G'$ of sodium montmorillonite dispersions reached a maximum at a critical $\mathrm{pH}_{crit}$ (in their work, $\mathrm{pH}_{crit}$=4), due to the formation of ordered edge-to-edge clusters. They argued that at pH<$\mathrm{pH}_{crit}$, the storage modulus was lower due to the formation of disordered house-of-cards clusters. Similar observations were made by Sohm and Tadros (1989) for commercial sodium-montmorillonite, and by Benna et al (1999) on three different sodium bentonite dispersions. The presence of clusters with different configurations as a function of the pH was also confirmed through small-angle X-ray scattering by Saunders et al (1999). For our G-O dispersions, pH$\sim$ 2 were measured for $1 < \phi/\phi_c < 5$, and pH= 5.15 at $\phi/\phi_c = 25$ (Table 1), implying a possible transition between two different microstructural configurations. Possibly, G-O could be arranged in a house-of-cards configuration when $1 < \phi/\phi_c < 5$, and in a "edge-to-edge" configuration when $\phi/\phi_c = 25$.

However, we cannot draw any conclusion from the pH data only. Further discussion based on rheological measurements is given in Section 3.2 and Section 3.3.

The linear oscillatory shear measurement investigates $G'$ and $G''$ as a function of angular frequency $\omega$ at imposed low shear deformation (frequency sweep). We carried out frequency sweep on aqueous G-O dispersions at $0.5 < \phi/\phi_c < 44$ with an imposed deformation $\gamma = 0.1$ % (see Figure 2(c-d)). When $\phi/\phi_c \geq 25$, both the storage and the loss moduli are almost independent of the angular frequency in the range of $1 < \omega < 100$ rad/s. When $\phi/\phi_c \leq 5$, both $G'$ and $G''$ show a dependence on the angular frequency when $\omega < 1$ rad/s. Similar behaviour in G-O dispersions has been reported by Vasu et al (2013) and Vallés et al (2014). Clusters made of G-O sheets show remarkable elasticity despite the low volume concentration, and elastic components always overcome viscous components at $\phi/\phi_c > 1$. We also observe a change of slope of $G'$ and $G''$ at $\phi = 0.08$ wt% ($\phi/\phi_c = 0.8$). This behaviour can be related to the transition from two different concentration regimes (Macosko (1994)), thus confirming our previous estimate of $\phi_c$ (discussed in Section 3.1.1).

### *3.2 Transient measurements of shear viscosity and first normal stress difference*

Aqueous graphene oxide dispersions show distinctive time-dependent phenomena. Vasu et al (2013) monitored the transient shear viscosity $\eta^+$ at different imposed stresses. For $\phi/\phi_c = 20$ and at an imposed stress $\tau = 0.1$ Pa, they reported strong oscillations in the shear viscosity, and a steady-state value for $\eta^+$ was never reached (they carried out measurements up to 1000 seconds). At the same concentration but at $\tau = 10$ Pa, steady-state value of $\eta^+$ was reached in $\sim 100$ s. This behaviour is very common for fluids with yield stresses such as aqueous G-O dispersions when $\phi/\phi_c > 1$ (Vasu et al (2013); Del Giudice and Shen (2017)). For fluids with a yield stress, transient experiments carried out by imposing a shear stress require very long times to reach a steady state value in $\eta^+$. Such experiments are then very valuable for determining the existence of an yield stress, but do not allow the evaluation of the shear viscosity value at steady-state.

We carried out transient measurements by imposing a shear rate $10^{-3} < \dot{\gamma} < 100\ s^{-1}$ and monitored $\eta^+$ over $t = 600$ s (Figure 3(a-d)), after a preshear $\dot{\gamma} = 1600\ \mathrm{s}^{-1}$ for 180 s. At $\phi/\phi_c = 44$, $\eta^+$ increases up to an average value $\eta \sim 10^5$ Pa·s. After $\sim 400$ s, transient viscosity $\eta^+$ oscillates between $7 \times 10^4 < \eta^+ < 2 \times 10^5$ Pa·s. When $\dot{\gamma} = 10^{-2}\ s^{-1}$, the dispersion displays a tiny overshoot in the viscosity that disappears

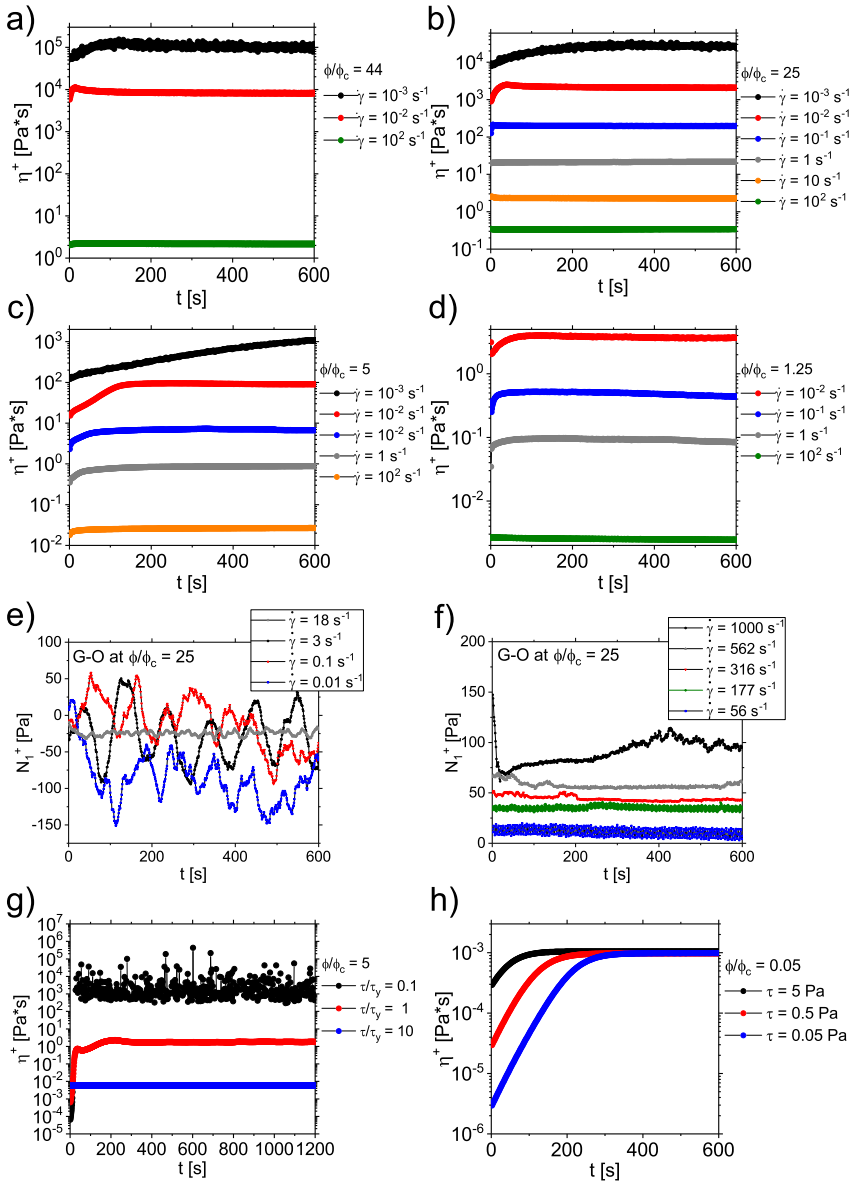


**Fig. 3 Transient viscosity $\eta^+$ reaches steady state on different time scales.** (a-d) Transient shear viscosity $\eta^+$ at different applied shear rates $\dot{\gamma}$ for G-O dispersion at concentrations (a) $\phi/\phi_c = 44$, (b) $\phi/\phi_c = 25$, (c) $\phi/\phi_c = 5$, (d) $\phi/\phi_c = 1.25$, with $\phi_c = 0.08$ wt%. A preshear $\dot{\gamma} = 1600\ s^{-1}$ for 180 s is applied prior to each measurements. **First Normal stress difference $N_1$ changes sign from positive to negative depending on the shear rate.** (e-f) Transient first normal stress difference $N_1^+$ at different applied shear rates $\dot{\gamma}$ for G-O dispersion at concentration $\phi/\phi_c = 25$. No preshear is applied. The full procedure is described in Section 2.4. **With applied stresses below the yield stress, transient viscosity $\eta^+$ displays strong oscillations.** (g-h) Transient shear viscosity at different applied shear stress $\tau$ for G-O dispersion at concentrations (d) $\phi/\phi_c = 5$ with $\tau_y = 0.9\ Pa$, (e) $\phi/\phi_c = 0.5$ (yield stress not detected). A preshear $\tau = 20\ Pa$ for 180 s is applied prior to each measurement.

almost immediately, but tiny oscillations are still observed. Even though steady-state is not fully achieved, an average value of the shear viscosity can be derived in the time interval of $200 < t < 600$ s (Figure 3a). At $\dot{\gamma} = 10^2\ s^{-1}$, aqueous G-O dispersion at $\phi/\phi_c = 44$ reaches a steady state value within 100 $s$. These results demonstrate that different time scales are required to reach steady-state, depending on the imposed shear rate. Owing to their morphology, G-O sheets experience significant Brownian diffusion (Vallés et al (2014)). At $\phi/\phi_c > 1$ and at low imposed shear rates, Brownian diffusion dominates convection forces. With increasing $\dot{\gamma}$, convection forces become comparable to Brownian forces and eventually dominate. The competing effects of Brownian diffusion and convection are quantified through the *Peclet number* $Pe$, defined as (Macosko (1994); Larson (1999)):

$$Pe = \frac{\dot{\gamma}}{\mathscr{D}_r}, \tag{2}$$

where $\dot{\gamma}$ is the applied shear rate, and $\mathscr{D}_r$ is the G-O sheet rotational diffusivity. Notice that rotational diffusivity is preferred to translational diffusivity due to the high anisotropy of G-O sheets. When $Pe < 1$, diffusion overcomes convection, and vice versa when $Pe > 1$. Rotational diffusivity for circular disk-like particle can be estimated as (Macosko (1994); Larson (1999)):

$$\mathscr{D}_r = \frac{3kT}{32\eta_s a^3} \sim 2\ s^{-1}, \tag{3}$$

where $k = 1.38 \times 10^{-23}$ J/K is the Boltzmann constant, $T = 295\ K$ the absolute temperature, $\eta_s = 10^{-3}$ Pa· s the viscosity of the solvent (water in our case), and $a = 0.58\ \mu$m is the average lateral radius of G-O sheets as obtained from AFM (see Figure 1). For $\dot{\gamma} = 10^{-3}\ s^{-1}$, $\dot{\gamma} = 10^{-2}\ s^{-1}$, and $\dot{\gamma} = 10^2\ s^{-1}$, Peclet numbers are $Pe \sim 5 \times 10^{-4}$, $Pe \sim 5 \times 10^{-3}$, and $Pe \sim 50$, respectively. At $\phi/\phi_c \geq 25$, at $Pe \sim 5 \times 10^{-4}$ and $Pe \sim 5 \times 10^{-3}$, we also observe oscillations of $\eta^+$ over time, and the transient shear viscosity $\eta^+$ does not approach a clear steady-state value (Figure 3b and Figure S4). At $1.25 < \phi/\phi_c < 5$, and at Peclet numbers $Pe < 1$, we observe long transients before reaching steady-state, while at shear rates such that $Pe > 1$, steady-state is reached in less than $\sim 100\ s$ (Figure 3(a-d)).

Results presented above agree well with those of laponite dispersions reported in the literature. Abou et al (2003) reported the effect of the imposed shear rate on the transient viscosity $\eta^+$ for laponite aqueous dispersions at 1.5 wt% (the value of the critical concentration $\phi_c$ was not provided). They found that at the lowest shear rate investigated $\dot{\gamma} = 50\ s^{-1}$, transient viscosity reached a steady state value after 50 hours, while increasing the imposed shear rate to $\dot{\gamma} = 500\ s^{-1}$, the equilibration time of $\eta^+$ dropped

to 1 hour. We observe similar behaviour (even though the absolute values of the shear rate are different) at $\phi/\phi_c > 1$, where the equilibration time of $\eta^+$ cannot be estimated when $Pe < 1$, but obtained at $\sim 100\ s$ when $Pe > 1$. The reduction of the equilibration time of $\eta^+$ with increasing shear rates is also in agreement with other theoretical models for glassy systems (i.e., systems of spherical particles at concentrations above $\phi_c$) (Cugliandolo et al (1997); Berthier et al (2000); Barrat and Berthier (2000)).

The oscillations of the transient viscosity $\eta^+$ (or of the transient shear stress) observed at $\phi/\phi_c \geq 25$ are also predicted to occur for nematic polymeric liquid crystals (Marrucci and Maffettone (1990a,b); Larson (1990)). Please note that the comparison between our data and the rheology of nematic polymeric liquid crystals is justified by several findings available in the literature. For instance, Xu and Gao (2011) carried out polarized microscopy images of graphene oxide dispersions at $0.1 < \phi/\phi_c < 2$. They found the existence of a stable nematic phase when $\phi/\phi_c > 1$. Similar results were also found by Yang et al (2013) using scanning electron microscopy. Moreover, Naficy et al (2014) observed the occurrence of nematic phases, by carrying out both rheological (oscillatory shear experiments) and cross-polarized microscopy measurements. The literature available regarding liquid crystal is enormous, and we will refer only to a very small part of it. We now compare our results to theoretical models on the rheological behavior of nematic polymeric liquid crystals. In particular, Marrucci and Maffettone (1990a,b) used a 2-dimensional theoretical model to predict shear stress oscillations over time for elongated rods, at low values of the shear rate. Such oscillations were ascribed to two possible mechanisms, termed as *tumbling* and *wagging*. The tumbling occurs at very low shear rates, and the average direction of the polymeric liquid crystal in the nematic phase changes continuously along the *vorticity* flow direction. The wagging, instead, occurs at slightly higher shear rates, and the average direction of the nematic phase oscillates between two angles along the *flow* direction. These findings were also confirmed by Larson (1990) using a 3D model. Currently, we cannot assess whether tumbling or wagging is responsible for the oscillations of $\eta^+$ observed at $Pe \sim 5 \times 10^{-4}$, since we ignore the value of the critical shear rate for the transition from tumbling to wagging. Further information can be derived from the analysis of the transient first normal stress difference $N_1^+$. Indeed, for nematic polymeric liquid crystals, it has been reported (Marrucci and Maffettone (1990a); Larson (1990)) that tumbling is correlated with *positive* values of $N_1$, while wagging is correlated with *negative* values of $N_1$, both at low shear rates. We observe negative values of the transient first normal stress difference $N_1^+$ in the range of shear rates $0.01 < \dot{\gamma} < 32\ s^{-1}$ (see some examples in

Figure 3e), thus implying the presence of wagging in the G-O dispersion at $\phi/\phi_c = 25$. Please note that our experimental data of $N_1$ should not be caused by the noise originated from the rheometer. Indeed, the stress applied by the rheometer to maintain the imposed shear rate $\dot{\gamma}$ is always above the measured yield stress (Figure S5). By increasing the shear rate to $\dot{\gamma} = 56\ s^{-1}$ and above, $N_1^+$ becomes positive and the oscillation is dampened compared with the case at lower $\dot{\gamma}$ (Figure 3f). The transition from negative to positive values of $N_1$ has also been reported for nematic polymeric liquid crystals. Kiss and Porter (1978) first observed this phenomenon in a nematic poly ($\gamma$-benzyl-glutamate) liquid crystal, which was later explained in terms of transition between tumbling-to-wagging and wagging-to-steady-state (Marrucci and Maffettone (1989, 1990a,b); Larson (1990)). Remarkably, our results on $N_1^+$ at $\dot{\gamma} > 56\ s^{-1}$ show steady-state conditions when $500 < t < 600\ s$, in agreement with experiments (Kiss and Porter (1978)) and theories (Marrucci and Maffettone (1990a,b); Larson (1990); Marrucci and Maffettone (1989)) reported on nematic polymeric liquid crystals. Our results are also consistent with a theoretical model recently presented by Schiller et al (2016), who proposed a mesoscopic theoretical approach to model the first normal stress difference in sheared kaolin suspensions. They suggested that a stationary flow alignment of kaolin sheets at low shear rate was not compatible with first negative normal stress difference. They concluded that negative first normal stress difference were due to tumbling (or wagging) of platelets at low shear rates. We indeed find positive values of the first normal stress difference only when steady-state is achieved, while negative $N_1^+$ are observed before $N_1^+$ reaches steady-state. We also observe tiny oscillations of the transient shear viscosity $\eta^+$ over time for $\dot{\gamma} = 10^{-2}$ (Figure S4). Such oscillations in $\eta^+$ are predicted to be less pronounced than that for $N_1^+$ in the wagging regime (Marrucci and Maffettone (1990a)).

Negative values of the first normal stress difference can also be ascribed to the formation of clusters of G-O sheets along the vorticity direction, in analogy with those observed for weakly attractive colloids. For instance, Montesi et al (2004) found negative normal stress difference for Newtonian attractive emulsion above the colloidal glass transition. Similar results were also found by Lin-Gibson et al (2004) for sheared carbon nanotube at $\phi/\phi_c > 1$. Clusters along the vorticity direction were also reported by Osuji and Weitz (2008) on shear thickening attractive colloidal system, and by Pignon et al (1997a) for shear thickening clay dispersions above the gel transition. It is worth noticing that Montesi et al (2004) suggested an

underlying analogy between clusters' formation along the vorticity direction and the nematic phase in polymeric liquid crystals. However, a clear understanding of such similarity is yet to be achieved.

We also adopt the approach used by Vasu et al (2013), and carry out transient viscosity measurements at $\phi/\phi_c = 5$ with imposed shear stress $\tau$ when $\tau/\tau_y = 0.1$, $\tau/\tau_y = 1$, $\tau/\tau_y = 10$, with $\tau_y = 0.9$ Pa, see Figure 3g (yield stress $\tau_y$ was derived through oscillatory measurements, Figure 2a). Transient viscosity $\eta^+$ shows strong oscillations when $\tau/\tau_y = 0.1$. Moreover, some negative values of $\eta^+$ are detected by the rheometer, confirming the existence of an yield stress in oscillatory shear experiments, consistent with those reported in literature (Vasu et al (2013); Vallés et al (2014)). In other words, such oscillations at $\tau/\tau_y = 0.1$ are the results of the noise coming from the rheometer, since the is stationary. At $\tau/\tau_y = 1$, a transient $\eta^+$ is found over the first 200 s, while at $\tau/\tau_y = 10$, $\eta^+$ reaches steady state within 100 s. Finally, yield stress is not expected when $\phi/\phi_c < 1$. Indeed, transient experiments at $\phi/\phi_c = 0.05$ do not exhibit any oscillations of $\eta^+$ for $0.05 < \tau < 5$ Pa (Figure 3h), in agreement with the findings of Vasu et al (2013).

### *3.3 Steady shear measurements to determine steady-state shear viscosity $\eta$ and first normal stress difference $N_1$*

Transient measurements allow us to determine the time scales involved to measure shear viscosity under steady-state conditions. With this in mind, we measure steady shear viscosity as follows. When $\phi/\phi_c > 1$ and $10^{-3} < \dot{\gamma} < 1\ s^{-1}$, we derive an experimental data point of $\eta$ every 300 s, because steady-state conditions are reached at around 300 s (Figure 3(a-d)). Recall that at $\phi/\phi_c \geq 5$ and $\dot{\gamma} \leq 10^{-2}\ s^{-1}$, steady state is not perfectly achieved, the data point evaluated represents an average reading. At $1 < \dot{\gamma} < 10^3\ s^{-1}$ experimental points are collected after 100 s, when steady-state conditions have been reached (Figure 3(a-d)). At $\phi/\phi_c < 1$ data are evaluated every 100 s in the whole range of shear rates investigated $1 < \dot{\gamma} < 1000\ s^{-1}$. At $\phi/\phi_c < 1$ and below $\dot{\gamma} = 1\ s^{-1}$, data are not reported because we reach the sensitivity limit of the rheometer. When $\phi/\phi_c > 1$, instead, data can be derived even at $10^{-3} < \dot{\gamma} < 1\ s^{-1}$ because the presence of clusters enhances the signal detectable by the rheometer. Due to the long time involved to carry out shear rheology measurements, any possible effects caused by the sedimentation of G-O sheets should also be considered. As reported by Larson (1999), sedimentation tends to occur when the ratio of gravitational to Brownian forces $a^4 \Delta\rho g / k_b T > 1$, where $a$ is the radius of the object, $\Delta\rho$ is the difference

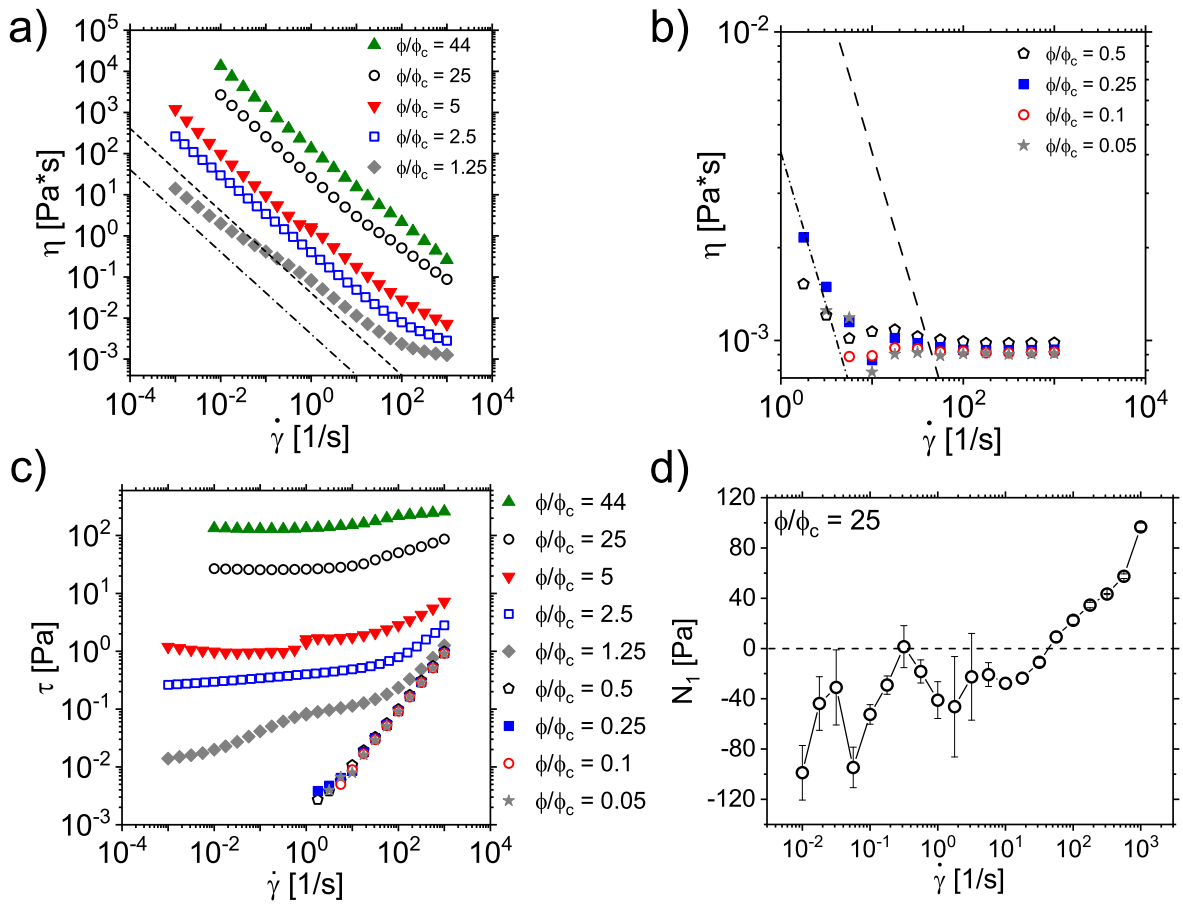


**Fig. 4 G-O dispersions above the critical concentration $\phi_c$ display strong shear-thinning with a yield stress.** Shear-viscosity $\eta$ as a function of the imposed shear rate $\dot{\gamma}$ for aqueous G-O dispersion in the range of $1.25 < \phi/\phi_c < 45$ (a), and $0.05 < \phi/\phi_c < 0.5$ (b), with $\phi_c = 0.08$ wt%. Dashed-dotted line and dashed lines in (a) and (b) represent the minimum value of viscosity $\eta_{min}$ detectable by the rheometer (due to the low-torque limit, as reported by Macosko (1994); Ewoldt et al (2015)) with $\eta_{min} = 2T_{min}/(\pi R^3\dot{\gamma})$, where $T_{min}$ is the minimum torque detectable, $R = 25$ mm is the plate diameter, and $\dot{\gamma}$ is the shear rate. Dashed line is $\eta_{min}$ for $T_{min} = 1$ $\mu$N·m, while dashed-dotted line is $\eta_{min}$ for $T_{min} = 0.1$ $\mu$N·m(c) The same data as in (a) and (b) plotted as shear stress $\tau$ versus shear rate $\dot{\gamma}$. Yield stress $\tau_y$ can be identified only when $\phi/\phi_c \geq 1$. A preshear $\dot{\gamma} = 1600\ s^{-1}$ for 180 s is applied prior to each measurement. **First Normal stress difference $N_1$ changes its sign from positive to negative depending on the shear rate.** (d) $N_1$ as a function of the imposed shear rate $\dot{\gamma}$ for aqueous G-O dispersion at $\phi/\phi_c = 25$. Each data point is obtained from transient $N_1^+$ measurement, averaging the last 100 seconds. No preshear is applied prior to each measurement.

between the density of the solvent and the dispersion, $g$ is the gravitational constant, $k_b$ is the Boltzmann constant and $T$ is the absolute temperature. The density measured by the G-O manufacturer falls in the range $1000 < \rho_{\text{G-O}} < 2000$ kg/m$^3$. Singh et al (2014) used a pycnometer and obtained the density of

G-O at $\rho_{\text{G-O}} \sim 2200$ kg/m$^3$. Sun et al (2010) report a value of $\rho_{G-O} = 1320$ Kg/m$^3$. Here we use the conservative upper limit of $\rho_{\text{G-O}} \sim 2200$ Kg/m$^3$. Consequently, $\Delta\rho = 1200$ Kg/m$^3$, and the upper limit of value $a^4\Delta\rho g/k_bT = 0.33$, thus no sedimentation is expected. Notice also that sedimentation in G-O dispersion was found to be negligible in previous reports (Vasu et al (2013)).

When $\phi/\phi_c > 1$, shear viscosity $\eta$ drastically decreases with the shear rate range $10^{-3} < \dot{\gamma} < 10\ s^{-1}$ investigated, exhibiting *shear-thinning* behaviour (Figure 4a). When $\phi/\phi_c < 1$, viscosity is largely constant for $\dot{\gamma} > 20\ s^{-1}$ (Figure 4b) because no interactions between G-O sheets are present; thus, isolated sheets align immediately along the flow direction (Del Giudice and Shen (2017)). A slight shear-thinning trend is instead present when $\dot{\gamma} < 20\ s^{-1}$, also reported by Tesfai et al (2013). However, the observed shear-thinning behaviour at $\phi/\phi_c < 1$ can be an artifact related to the low-torque limit (Macosko (1994); Ewoldt et al (2015)). The minimum value of viscosity $\eta_{min}$ dictated by the low-torque limit can be evaluated for parallel plate geometry as (Macosko (1994); Ewoldt et al (2015)):

$$\eta_{min} = \frac{2T_{min}}{\pi R^3 \dot{\gamma}}, \tag{4}$$

where $T_{min}$ is the minimum torque detectable, $R = 25$ mm is the plate diameter, and $\dot{\gamma}$ is the shear rate. Dashed line of Figure 4(a-b) is $\eta_{min}$ for $T_{min} = 1\ \mu$N·m, while dashed-dotted line is $\eta_{min}$ for $T_{min} = 0.1\ \mu$N·m. For our rheometer (Anton Paar MCR502), the lowest detectable torque by technical specification is $T_{min} = 0.1\ \mu$N·m (dashed-dotted line in Figure 4(a-b)). However, a more conservative value for the torque is $T_{min} = 1\ \mu$N·m (dashed line in Figure 4(a-b)). Therefore, the observed shear-thinning can be the result of an artifact. Our data in the concentration range $\phi/\phi_c < 1$ are also in agreement with other existing findings on G-O dispersions (Tesfai et al (2013); Vallés et al (2014)).

Shear viscosity $\eta$ of aqueous G-O dispersions increases monotonically with increasing $\phi/\phi_c$ across the whole range of shear rate $10^{-3} < \dot{\gamma} < 10\ s^{-1}$ investigated (Figure 4(a-b)). Vallés et al (2014) performed similar experiments and found that $\eta$ was monotonic within the concentration range $1 < \phi/\phi_c < 267$. Kumar et al (2014), instead, reported a non-monotonic behaviour of $\eta$ with the concentration $0.6 < \phi/\phi_c < 1.2$. Since our results suggest the existence of a nematic phase in the G-O dispersion at $\phi/\phi_c = 25$, the isotropic to nematic transition should fall in the concentration range of $5 < \phi/\phi_c < 25$. An estimate of the nematic concentration is $\phi_{nematic} = 6.8/\alpha = 0.58$ vol% (Aboutalebi et al (2011); Eppenga and Frenkel (1984)), where $\alpha = 2a/d \sim 1160$ is the aspect ratio. Assuming a G-O density of $\rho_g = 2200$ Kg/m$^3$, we obtain a mass concentration of 1.28 wt%, that is $\phi/\phi_c \sim 16$.

Steady shear viscosity data can also be plotted as shear stress $\tau$ against shear rate $\dot{\gamma}$ (Figure 4c). When $2.5 < \phi/\phi_c < 44$, shear stress $\tau$ is almost independent of the shear rate $\dot{\gamma}$, confirming the existence of the yield stress for aqueous G-O dispersions. At $\phi/\phi_c = 1.25$, a slight dependence of $\tau$ can be observed and the plateau region becomes less pronounced, probably because of the proximity to the critical concentration $\phi_c$. When $\phi/\phi_c < 1$, aqueous G-O dispersions behave like a simple Newtonian liquid when $\dot{\gamma} > 60\ s^{-1}$.

Our steady shear data are also in qualitative agreement with previous works on organoclays and laponite dispersions. In particular, Hato et al (2011) observed both shear-thinning and yield stress behaviour for a 20 wt% dispersion of clays in silicon oil (no values of $\phi_c$ were provided). Similar results were also reported by King Jr et al (2007) on aqueous dispersions of cloisite organoclays, by Kimura et al (2011) on hectorite (plate-like clay) particles dispersed in deionized water, and by Bekkour et al (2005) on aqueous dispersions of bentonite (plate-like clays).

Reproducibility of our experimental data has also been verified by carrying out experiments with cone and plate fixtures, and by repeating the experiments with parallel plates at $\phi/\phi_c = 5$ and $\phi/\phi_c = 25$ (See Figure S6 and Figure S7).

Values of the first normal stress difference $N_1$ at a given shear rate $\dot{\gamma}$ (Figure 4d) are derived from transient measurements (Figure 3(e-f)) by averaging the experimental points in the last 100 seconds. We clearly observe the transition from negative to positive value of $N_1$ at a critical shear rate $\dot{\gamma}_c = 56\ s^{-1}$. Moreover, at $\dot{\gamma} > \dot{\gamma}_c$ experimental data exhibit smaller standard deviations when compared to data collected at $\dot{\gamma} < \dot{\gamma}_c$. Indeed, steady-state regime is achieved at $\dot{\gamma} > \dot{\gamma}_c$, while the wagging (i.e., when $N_1 < 0$) at $\dot{\gamma} < \dot{\gamma}_c$ leads to oscillations in $N_1$, resulting in a wider standard deviation. Notice also that, values of $N_1$ in the wagging regime collected under different shear rates are based on averaged readings, since steady-state has not been fully achieved. Negative values of $N_1$ were also observed by Niu et al (2014) on G-O sheets dispersed in oil. Niu et al (2014) employed parallel plates geometry to measure the difference between first and second normal stress difference, $\Delta N$. They did not observe a clear transition from negative to positive values of $\Delta N$. Comparison between our data and those of Niu et al (2014) suggest an effect of the second normal stress difference $N_2$ on the rheology of the system. Lin-Gibson et al (2004) observed negative values of $\Delta N$ over time for nanotube dispersions. They ascribed this result to the alignment of carbon nanotubes clusters along the vorticity direction. Finally, Moan et al (2003) also observed negative values of $N_1$ for dispersions of plate-like kaolin particles. They drew analogies

between their findings and the tumbling in polymeric liquid crystals. Transition from negative to positive values of $\Delta N$ were also observed by Il Jun and Sang Lee (2012) on G-O/polycarbonate composites.

## 4 Conclusions

In this work we have performed detailed rheological characterisations of aqueous G-O dispersions in the concentration range of $0.05 < \phi/\phi_c < 44$ ($\phi_c = 0.08$ wt%), aiming to fill the gap between transient and steady shear rheology of aqueous G-O dispersions. G-O sheets analyzed through AFM images are heterogeneous both in their sizes and shapes, with an average lateral radius $a = 0.58 \pm 0.4$ $\mu$m and a thickness $d \sim 1$ nm. Owing to the heterogeneity of the dispersions, the critical concentration $\phi_c = 0.08$ wt% is determined using oscillatory shear measurements. Aqueous G-O dispersions show distinct elastic behaviour when $\phi/\phi_c > 1$, due to the formation of G-O sheets clusters (Vasu et al (2013); Del Giudice and Shen (2017)). Yield stress $\tau_y$ is determined from amplitude sweep measurements for G-O dispersions at $1 < \phi/\phi_c < 44$. We find $\tau_y \propto \phi/\phi_c^{2.35\pm0.86}$, in good agreement with other works reported on G-O dispersions (Vasu et al (2013); Kumar et al (2014)), on laponite dispersions (Pignon et al (1997b)) and organoclays (King Jr et al (2007)).

Steady-state conditions are identified from transient measurements at $1 < \phi/\phi_c < 44$ and for different imposed shear rates $\dot{\gamma}$. In transient measurements, different trends are displayed at different Peclet number $Pe$. At $Pe \sim 5 \times 10^{-4}$, transient viscosity $\eta^+$ shows fluctuations over time, and steady-state is not clearly reached. When $Pe \sim 5 \times 10^{-3}$, steady-state is approached after $\sim 300$ s, while at higher $Pe$ steady state is approached after $\sim 200$ s ($10^{-2} < Pe < 1$) or $\sim 100$ s ($Pe > 1$). Stress-imposed measurements confirm the existence of yield stress when $\phi/\phi_c > 1$, in agreement with other works (Vasu et al (2013); Vallés et al (2014)). At $\phi/\phi_c = 25$, transient measurements of the first normal stress difference suggest that G-O dispersion behave like nematic polymeric liquid crystals.

Steady-shear measurements show the presence of a strong shear-thinning trend when $\phi/\phi_c > 1$, in agreements with experimental measurements reported on aqueous G-O dispersions (Vallés et al (2014)), laponite dispersions (Abou et al (2003); Labanda et al (2007)), organoclay dispersions (King Jr et al (2007); Hato et al (2011); Kimura et al (2011); Bekkour et al (2005)), and also with theoretical models for nematic polymeric liquid crystals (Larson (1999)). We also report the first evidence of transition from negative to positive values of $N_1$ for aqueous G-O dispersions.

Future efforts should be devoted to preparing uniformly sized G-O sheets for both applied research and material characterizations purposes. Sample heterogeneity makes comparisons between different measurements very difficult, and does not permit definitive conclusions regarding flow behaviour of aqueous G-O dispersions, thus making the operation conditions of G-O materials difficult to control. The analogy between the rheology of aqueous G-O dispersions and of clay dispersions (or dispersions of other 2D systems) also deserve further investigations. Indeed, a general theoretical framework is desirable to describe the rheological behaviour of such anisotropic systems. Further investigations of the transient first normal stress difference at higher values of $\phi/\phi_c$ would be beneficial to understand the similarities between G-O dispersions and nematic polymeric liquid crystals. Investigation of the effect of wall slip on the rheology of G-O dispersions would also be beneficial. In fact, to the best of our knowledge, only Vasu et al (2013) examined the problem, and reported that wall slip was not significant in Couette flow. However, a characterization of wall slip in geometries such as parallel plates or cone and plates is still missing. The effect of pH on the rheological properties of G-O dispersions can tune materials with optimised mechanical properties, induced by ordered edge-to-edge structures. Addition of salts or surfactants can clarify the interactions occurring between dispersed G-O sheets. Finally, dilute polymer solutions could also be adopted as solvents for G-O sheets. Indeed, polymer solutions have been reported to "trigger" a variety of phenomena in particle suspensions (D'Avino and Maffettone (2015)), and can advance new exciting applications of carbon-related materials.

*Acknowledgements* The authors thank Dr. Steven Aird for careful proof reading. The authors also thank Prof. Pier Luca Maffettone, Prof. Giovanniantonio Natale, and Prof. Gareth McKinley for helpful discussions. F.D.G. and A.Q.S. gratefully acknowledge the support of the Okinawa Institute of Science and Technology Graduate University with subsidy funding from the Cabinet Office, Government of Japan. B.V.C. and R.S.R acknowledge the support of the Institute for Basic Science (IBS-R019-D1).

## References

Abou B, Bonn D, Meunier J (2003) Nonlinear rheology of laponite suspensions under an external drive. Journal of Rheology 47(4):979–988

Aboutalebi SH, Gudarzi MM, Zheng QB, Kim JK (2011) Spontaneous formation of liquid crystals in ultralarge graphene oxide dispersions. Advanced Functional Materials 21(15):2978–2988

Akbari A, Sheath P, Martin ST, Shinde DB, Shaibani M, Banerjee PC, Tkacz R, Bhattacharyya D, Majumder M (2016) Large-area graphene-based nanofiltration membranes by shear alignment of discotic nematic liquid crystals of graphene oxide. Nature communications 7

Bai H, Li C, Wang X, Shi G (2011) On the gelation of graphene oxide. J Phys Chem C 115(13):5545–5551

Barnes HA, Hutton JF, Walters K (1989) An introduction to rheology, vol 3. Elsevier

Barrat JL, Berthier L (2000) Fluctuation-dissipation relation in a sheared fluid. Physical Review E 63(1):012,503

Bekkour K, Leyama M, Benchabane A, Scrivener O (2005) Time-dependent rheological behavior of bentonite suspensions: An experimental study. Journal of Rheology 49(6):1329–1345

Benna M, Kbir-Ariguib N, Magnin A, Bergaya F (1999) Effect of ph on rheological properties of purified sodium bentonite suspensions. Journal of Colloid and Interface Science 218(2):442–455

Berthier L, Barrat JL, Kurchan J (2000) A two-time-scale, two-temperature scenario for nonlinear rheology. Physical Review E 61(5):5464

Chatterjee T, Krishnamoorti R (2013) Rheology of polymer carbon nanotubes composites. Soft Matter 9(40):9515–9529

Cocchini F, Nobile M, Acierno D (1992) Letter: About negative first normal stress differences in a thermotropic l.c. polymer. J Rheol 36:1307–1311

Cugliandolo LF, Kurchan J, Peliti L (1997) Energy flow, partial equilibration, and effective temperatures in systems with slow dynamics. Physical Review E 55(4):3898

Das S, Irin F, Ma L, Bhattacharia SK, Hedden RC, Green MJ (2013) Rheology and morphology of pristine graphene/polyacrylamide gels. ACS Appl Mater Interfaces 5(17):8633–8640

D'Avino G, Maffettone P (2015) Particle dynamics in viscoelastic liquids. J Non-Newton Fluid 215:80–104

Del Giudice F, Shen AQ (2017) Shear rheology of graphene oxide dispersions. Curr Opin Chem Eng 16C:23–30

Dinkgreve M, Paredes J, Denn MM, Bonn D (2016) On different ways of measuring "the" yield stress. Journal of Non-Newtonian Fluid Mechanics 238:233–241

Dreyer DR, Park S, Bielawski CW, Ruoff RS (2010) The chemistry of graphene oxide. Chem Soc Rev 39(1):228–240

Eppenga R, Frenkel D (1984) Monte carlo study of the isotropic and nematic phases of infinitely thin hard platelets. Molecular physics 52(6):1303–1334

Ewoldt RH, Johnston MT, Caretta LM (2015) Experimental challenges of shear rheology: how to avoid bad data. In: Complex Fluids in Biological Systems, Springer, pp 207–241

Geim AK, Novoselov KS (2007) The rise of graphene. Nat Mater 6(3):183–191

Green MJ, Behabtu N, Pasquali M, Adams WW (2009) Nanotubes as polymers. Polymer 50(21):4979–4997

Guimont A, Beyou E, Martin G, Sonntag P, Cassagnau P (2011) Viscoelasticity of graphite oxide-based suspensions in pdms. Macromolecules 44(10):3893–3900

Hato MJ, Zhang K, Ray SS, Choi HJ (2011) Rheology of organoclay suspension. Colloid and Polymer Science 289(10):1119

Hobbie EK (2010) Shear rheology of carbon nanotube suspensions. Rheologica acta 49(4):323–334

Il Jun S, Sang Lee H (2012) Negative normal stress differences in graphene/polycarbonate composites. Applied Physics Letters 100(16):164,108

Khandal R, Tadros TF (1988) Application of viscoelastic measurements to the investigation of the swelling of sodium montmorillonite suspensions. Journal of colloid and interface science 125(1):122–128

Kim H, Macosko CW (2009) Processing-property relationships of polycarbonate/graphene composites. Polymer 50(15):3797–3809

Kim JE, Lee HS (2014) Oscillatory shear induced gelation of graphene–poly (vinyl alcohol) composite hydrogels and rheological premonitor of ultra-light aerogels. Polymer 55(1):287–294

Kimura H, Sakurai M, Sugiyama T, Tsuchida A, Okubo T, Masuko T (2011) Dispersion state and rheology of hectorite particles in water over a broad range of salt and particle concentrations. Rheologica acta 50(2):159–168

King Jr H, Milner ST, Lin MY, Singh JP, Mason T (2007) Structure and rheology of organoclay suspensions. Physical Review E 75(2):021,403

Kiss G, Porter RS (1978) Rheology of concentrated solutions of poly ($\gamma$-benzyl-glutamate). In: Journal of Polymer Science: Polymer Symposia, Wiley Online Library, vol 65, pp 193–211

Krieger IM, Dougherty TJ (1959) A mechanism for non-newtonian flow in suspensions of rigid spheres. Transactions of The Society of Rheology (1957-1977) 3(1):137–152

Kugge C, Vanderhoek N, Bousfield D (2011) Oscillatory shear response of moisture barrier coatings containing clay of different shape factor. Journal of colloid and interface science 358(1):25–31

Kumar P, Maiti UN, Lee KE, Kim SO (2014) Rheological properties of graphene oxide liquid crystal. Carbon 80:453–461

Labanda J, Sabaté J, Llorens J (2007) Rheology changes of laponite aqueous dispersions due to the addition of sodium polyacrylates of different molecular weights. Colloids and Surfaces A: Physicochemical and Engineering Aspects 301(1):8–15

Larson R (1990) Arrested tumbling in shearing flows of liquid-crystal polymers. Macromolecules 23(17):3983–3992

Larson RG (1999) The structure and rheology of complex fluids, vol 150. Oxford university press New York

Li D, Müller MB, Gilje S, Kaner RB, Wallace GG (2008) Processable aqueous dispersions of graphene nanosheets. Nature nanotechnology 3(2):101–105

Lin-Gibson S, Pathak J, Grulke E, Wang H, Hobbie E (2004) Elastic flow instability in nanotube suspensions. Physical review letters 92(4):048,302

Liu J, Chen G, Jiang M (2011) Supramolecular hybrid hydrogels from noncovalently functionalized graphene with block copolymers. Macromolecules 44(19):7682–7691

Liu Y, Chen C, Liu L, Zhu G, Kong Q, Hao R, Tan W (2015) Rheological behavior of high concentrated dispersions of graphite oxide. Soft Materials 13(3):167–175

Lu C, Mai YW (2005) Influence of aspect ratio on barrier properties of polymer-clay nanocomposites. Phys Rev Lett 95(8):088,303

Macosko C (1994) Rheology: Principles, measurements, and applications. 1994. Wiley-VCH

Marrucci G, Maffettone P (1989) A description of the liquid-crystalline phase of rodlike polymers at high shear rates. Macromolecules 22(10):4076–4082

Marrucci G, Maffettone P (1990a) Nematic phase of rodlike polymers. i. prediction of transient behavior at high shear rates. Journal of rheology 34(8):1217–1230

Marrucci G, Maffettone P (1990b) Nematic phase of rodlike polymers. ii. polydomain predictions in the tumbling regime. Journal of rheology 34(8):1231–1244

Michot LJ, Bihannic I, Maddi S, Funari SS, Baravian C, Levitz P, Davidson P (2006) Liquid–crystalline aqueous clay suspensions. Proceedings of the National Academy of Sciences 103(44):16,101–16,104

Moan M, Aubry T, Bossard F (2003) Nonlinear behavior of very concentrated suspensions of plate-like kaolin particles in shear flow. Journal of Rheology 47(6):1493–1504

Montesi A, Peña AA, Pasquali M (2004) Vorticity alignment and negative normal stresses in sheared attractive emulsions. Physical Review Letters 92(5):058,303

Naficy S, Jalili R, Aboutalebi SH, Gorkin III RA, Konstantinov K, Innis PC, Spinks GM, Poulin P, Wallace GG (2014) Graphene oxide dispersions: tuning rheology to enable fabrication. Materials Horizons 1(3):326–331

Niu R, Gong J, Xu D, Tang T, Sun ZY (2014) Influence of molecular weight of polymer matrix on the structure and rheological properties of graphene oxide/polydimethylsiloxane composites. Polymer 55(21):5445–5453

Niu X, Gong J, Xu D, Tanga T, Sun ZY (2015) Impact of particle surface chemistry on the structure and rheological properties of graphene-based particle/polydimethylsiloxane composites. RSC Adv 5:34,885–34,893

Onsager L (1949) The effects of shape on the interaction of colloidal particles. Annals of the New York Academy of Sciences 51(4):627–659

Osuji CO, Weitz DA (2008) Highly anisotropic vorticity aligned structures in a shear thickening attractive colloidal system. Soft Matter 4(7):1388–1392

Park S, Ruoff RS (2009) Chemical methods for the production of graphenes. Nature nanotechnology 4(4):217–224

Perge C, Taberlet N, Gibaud T, Manneville S (2014) Time dependence in large amplitude oscillatory shear: A rheo-ultrasonic study of fatigue dynamics in a colloidal gel. Journal of Rheology 58(5):1331–1357

Pignon F, Magnin A, Piau JM (1997a) Butterfly light scattering pattern and rheology of a sheared thixotropic clay gel. Physical Review Letters 79(23):4689

Pignon F, Magnin A, Piau JM, Cabane B, Lindner P, Diat O (1997b) Yield stress thixotropic clay suspension: Investigations of structure by light, neutron, and x-ray scattering. Physical Review E 56(3):3281

Potts JR, Dreyer DR, Bielawski CW, Ruoff RS (2011) Graphene-based polymer nanocomposites. Polymer 52(1):5–25

Renou F, Stellbrink J, Petekidis G (2010) Yielding processes in a colloidal glass of soft star-like micelles under large amplitude oscillatory shear (laos). Journal of Rheology 54(6):1219–1242

Sadasivuni KK, Ponnamma D, Kumar B, Strankowski M, Cardinaels R, Moldenaers P, Thomas S, Grohens Y (2014) Dielectric properties of modified graphene oxide filled polyurethane nanocomposites and its correlation with rheology. Compos Sci Technol 104:18–25

Saunders JM, Goodwin JW, Richardson RM, Vincent B (1999) A small-angle x-ray scattering study of the structure of aqueous laponite dispersions. The Journal of Physical Chemistry B 103(43):9211–9218

Schiller P, Bombrowski M, Wahab M, Mögel HJ (2016) Models for normal stress and orientational order in sheared kaolin suspensions. Journal of Rheology 60(2):311–325

Schweizer T, Bardow A (2006) The role of instrument compliance in normal force measurements of polymer melts. Rheol acta 45(4):393–402

Shaffer M, Windle A (1999) Analogies between polymer solutions and carbon nanotube dispersions. Macromolecules 32(20):6864–6866

Shih WY, Shih WH, Aksay IA (1999) Elastic and yield behavior of strongly flocculated colloids. Journal of the American Ceramic Society 82(3):616–624

Singh VK, Cura ME, Liu X, Johansson LS, Ge Y, Hannula SP (2014) Tuning the mechanical and adsorption properties of silica with graphene oxide. ChemPlusChem 79(10):1512–1522

Sohm R, Tadros TF (1989) Viscoelastic properties of sodium montmorillonite (gelwhite h) suspensions. Journal of Colloid and Interface Science 132(1):62–71

Sun X, Luo D, Liu J, Evans DG (2010) Monodisperse chemically modified graphene obtained by density gradient ultracentrifugal rate separation. Acs Nano 4(6):3381–3389

Tesfai W, Singh P, Shatilla Y, Iqbal MZ, Abdala AA (2013) Rheology and microstructure of dilute graphene oxide suspension. Journal of nanoparticle research 15(10):1–7

Tripathi SN, Malik RS, Choudhary V (2015) Melt rheology and thermomechanical behavior of poly (methyl methacrylate)/reduced graphene oxide nanocomposites. Polym Advan Technol 26(12):1558–1566

Vallés C, Young RJ, Lomax DJ, Kinloch IA (2014) The rheological behaviour of concentrated dispersions of graphene oxide. Journal of Materials Science 49(18):6311–6320

Vasu K, Krishnaswamy R, Sampath S, Sood A (2013) Yield stress, thixotropy and shear banding in a dilute aqueous suspension of few layer graphene oxide platelets. Soft Matter 9(25):5874–5882

Walters K (1975) Rheometry. Chapman & Hall London

Xu Z, Gao C (2011) Aqueous liquid crystals of graphene oxide. ACS Nano 5(4):2908–2915

Yang X, Guo C, Ji L, Li Y, Tu Y (2013) Liquid crystalline and shear-induced properties of an aqueous solution of graphene oxide sheets. Langmuir 29(25):8103–8107

Yao L, Lu Y, Wang Y, Hu L (2014) Effect of graphene oxide on the solution rheology and the film structure and properties of cellulose carbamate. Carbon 69:552–562